Mon. Not. R. Astron. Soc. **000**, 000–000 (0000) Printed 24 February 2014 (MN LATEX style file v2.2)

GRAVLITE: Non-parametric method for mass modelling of spherical systems

P. Steger[1⋆], J. I. Read[1,2], D. von Rickenbach[1]
[1] *Institute for Astronomy, Department of Physics, ETH Zürich, Wolfgang-Pauli-Strasse 27, CH-8093 Zürich, Switzerland*
[2] *Department of Physics, University of Surrey, Guildford, GU2 7XH, UK*

24 February 2014

ABSTRACT

We propose a new non-parametric method based on Jeans modelling to determine the mass distribution in spherical systems with a single or multiple tracer populations. A high dimensional parameter space encoding tracer density, line of sight velocity dispersion and total mass density is sampled with MultiNest.

Without assumptions on the functional form of any of these profiles, we can reproduce liably the total mass density of spherical mock dwarf galaxies, and start to disentangle the degeneracy between dark matter density and tracer velocity anisotropy.

We show applications to triaxial systems, and point out what characteristics of the data are required to detect cores of a given radius.

Key words: galaxies: dwarf – galaxies: fundamental parameters – galaxies: kinematics and dynamics – cosmology: dark matter

1 INTRODUCTION

Cosmological ΛCDM simulations of representative patches of the Universe predict the dark matter to assemble self-similarly. Assuming that only dark matter might influence the physics on all scales down to the stellar regime, Navarro et al. (1997) found that the density profiles of the resulting halos are best described by a function diverging as r^{-1} towards the center, turning over to r^{-2} at a scale radius, and falling off as r^{-3} towards infinity. The asymptotic value $\alpha = d\log\rho/d\log r = -1$ in the center is challenged by observations.

Observations of low surface brightness galaxies measure rotation curves and deduce from them a constant density – $\alpha = 0$ – below a rather large scale radius r_S (de Blok et al. 2001), (McGaugh et al. 2001), contrary to the theoretical predictions. This fact became known as the cusp/core problem.

Many solutions have been proposed. It was deemed probable that difficulties in data modelling prevent observations from resolving cusps. **(TODO: citation)**

Another solution was to propose that dark matter is not cold as assumed, but has a high streaming velocity with a warm component smearing out density peaks below a certain scale.

Dark matter could also be self-interacting, as e.g. postulated by (Spergel & Steinhardt (2000), Vogelsberger et al. (2012)), and have a large scattering cross-section and low annihilation or dissipation cross-section, and thus prevent formation of overly-dense cusps.

For the n-body simulations in question, it became clear that baryonic physics plays a crucial role for the buildup of the overall density profile on small scales, and thus dark matter.

In particular, modelling of stellar feedback, the introduction of a higher density threshold for star formation and an increase of resolution for treatment of individual star-forming regions in a cosmological context led simulations to reveal dwarf galaxies with shallow central density slopes in dark matter (Governato et al. 2010). This compares well with what is found in THINGS dwarf galaxies (Oh et al. 2011).

A possible way for clarification in this issue are dwarf spheroidal galaxies, lying relatively close to the Sun such that they can be resolved, often allowing us to observe individual stars. We need a method to model their mass distribution from the observations to investigate whether they exhibit a cusp or a core, and whether simulations are able to reproduce the dark matter distribution.

An early approach for mass modelling general triaxial systems in dynamical equilibrium was proposed by Schwarzschild (1979): Based on a postulated density profile and a corresponding gravitational potential, an ensemble of orbits are calculated and superposed to yield the underlying density profile.

Another mass modelling approach is to use the motion of globular clusters inside dwarf galaxies (Goerdt et al. 2006), (Cole et al. 2012). If the density distribution follows

⋆ E-mail: psteger@phys.ethz.ch

a cored profile, globular clusters will not fall in, or will even get pushed out of the core if they formed inside. In Fornax dSph, there is evidence for a core (Read et al. 2006).

Yet another method makes use of the Jeans equations encompassing tracer density, velocity dispersion and the gravitational potential to solve for the potential, and ultimately get the underlying dark matter density (Binney & Tremaine 2008). Mostly, a functional form with some free parameter(s) is assumed for the density profile, and fitting routines are used to yield the best agreeing form. While this can give good agreement on specific systems (**(TODO: cite King)**), it only ever allows the particular class of models to be fitted. A more elegant way would be to infer the functional form as well from the data, in a non-parametric way.

In this paper, we propose a new non-parametric mass-modelling technique based on the Jeans approach, with no assumptions on the functional form of the dark matter density, nor the velocity anisotropy profile. We sample all of these profiles in N_{bin} bins, and deduce the most likely profiles.

Our method has following advantages over other methods presented so far:

(i) no assumptions on the functional form of the underlying dark matter;
(ii) applicable to any gravitational model, since Jeans equation and Poisson equation are solved each on their own;
(iii) robust to noise in the data, as no numerical differentiation is used as soon as the three-dimensional density model is set up.

We cannot employ our method on all systems, though, as the strong assumption of spherical symmetry enters in a first step. Beware that dSph galaxies of the local group are known to be slightly non-spherical, with an average ellipticity of 0.3 (Mateo 1998).

We find at this early stage, as well, that we might be susceptible to the mass/velocity anisotropy, due to the following reason.

An assumption on the velocity anisotropy profile is required to get a mass density in the case of lowest-order Jeans equations. Since it is not known a priori and hard to measure observationally how much the system is supported by rotational motion, this leads to a degeneracy between mass and velocity anisotropy.

(TODO: put the following three paragraphs in Discussion?)

Walker & Peñarrubia (2011) split the stellar tracers of Fornax dSph into two populations with different metallicities and half-mass radii, and make use of the fact that the enclosed mass at the half-mass radius is independent of the underlying velocity anisotropy profile, to get two points in the center of the dwarf galaxy, from which constraints on the inner DM density slope can be drawn. One further line of investigation will show whether splitting into N populations might yield a better result with our method.

Higher order Jeans equations could help to break the degeneracy as well (Łokas 2002). As pointed out by (**? ?**), this might not be enough, as any additional order introduced more anisotropy parameters than they help to constrain. Introducing virial shape parameters yields a much better handle on the degeneracy.

Another degeneracy between inner DM slope and concentration shows up as well. With better data available for the local dSphs, distribution function based methods may be used.

2 METHOD

The collisionless Boltzmann equation for a spherical system with gravitational potential Φ,

$$\frac{\mathrm{d}f}{\mathrm{d}t} = \frac{\partial f}{\partial t} + \nabla_{\vec{x}} f \cdot \vec{v} - \nabla_{\vec{v}} f \cdot \nabla_{\vec{x}} \Phi = 0, \tag{1}$$

describes the motion of tracer stars at positions $\vec{x}$, with velocity $\vec{v}$, and with distribution function $f(\vec{x}, \vec{v})$.

In spherical coordinates (r, θ, ϕ), the collisionless Boltzmann equation then reads as

$$\frac{\partial f}{\partial t} + \dot{r}\frac{\partial f}{\partial r} + \dot{\theta}\frac{\partial f}{\partial \theta} + \dot{\phi}\frac{\partial f}{\partial \phi} + \dot{v}_r\frac{\partial f}{\partial v_r} + \dot{v}_\theta\frac{\partial f}{\partial v_\theta} + \dot{v}_\phi\frac{\partial f}{\partial v_\phi} = 0 \tag{2}$$

with velocities

$$\dot{r} = v_r, \tag{3}$$
$$\dot{\theta} = v_\theta / r \tag{4}$$
$$\dot{\phi} = v_\phi / r \sin\theta. \tag{5}$$

The assumption of steady state hydrodynamic equilibrium gives $\partial f/\partial t = 0$ and $\bar{v}_r = 0$, and using spherical symmetry $\bar{v}_\theta = 0$, $\bar{v}_\phi = 0$ with a unique tangential velocity dispersion $\sigma_\phi^2 = \sigma_\theta^2 = \sigma_t^2$ and a fourth order moment $\bar{v_r^4}$ we get

$$\frac{1}{\nu}\frac{\partial}{\partial r}(\nu\sigma_r^2) + 2\frac{\sigma_r^2 - \sigma_t^2}{r} = -\frac{\partial \Phi}{\partial r} = -\frac{GM(<r)}{r^2}, \tag{6}$$
$$\frac{\partial}{\partial r}(\nu\bar{v_r^4}) + \frac{2\beta}{r}\nu\bar{v_r^4} + 3\nu\sigma_r^2\frac{\partial \Phi}{\partial r} = 0, \tag{7}$$

with enclosed total mass $M(<r)$ inside radius r, density ν of any collection of tracer particles in the potential Φ, and gravitational constant $G = 6.67398 \cdot 10^{-11}\mathrm{m}^3/\mathrm{kg\,s}^2$. The departure from spherical hydrostatic equilibrium $\sigma_r^2 = \sigma_t^2$ is measured by the anisotropy parameter

$$\beta \equiv 1 - \frac{\sigma_t^2}{\sigma_r^2} \tag{8}$$

with values in the range from $-\infty$ (purely circular orbits) through 0 (hydrostatic equilibrium) to 1 (purely radial orbits).

Integrating both sides of equation 6 gives the radial velocity dispersion as function of the projected radius R, and correspondingly the fourth order moment,

$$\sigma_r^2(R) = \frac{1}{\nu(R)}\exp\left(-2\int_{r_{min}}^{R}\frac{\beta(s)}{s}\mathrm{d}s\right)\cdot \tag{9}$$
$$\int_R^\infty \frac{GM(r)\nu(r)}{r^2}\exp\left(2\int_{r_{min}}^{r}\frac{\beta(s)}{s}\mathrm{d}s\right)\mathrm{d}r.$$

$$\bar{v_r^4}(R) = \frac{3}{\nu(R)}\exp\left(-2\int_{r_{min}}^{R}\frac{\beta(s)}{s}\mathrm{d}s\right)\cdot$$

$$\int_R^\infty \frac{GM(r)\nu\sigma_r^2}{r^2} \exp\left(2\int_{r_{min}}^r \frac{\beta(s)}{s}\mathrm{d}s\right)\mathrm{d}r.$$

For distant spherical systems, only the projected velocity dispersion $\sigma_{\rm LOS}$ and the fourth order moment $v^{\bar{4}}_{\rm los}$ can be measured, which in our case is given by

$$\sigma^2_{\rm LOS}(R) = \frac{2}{\Sigma(R)}\int_R^\infty \left(1-\beta\frac{R^2}{r^2}\right)\frac{\nu(r)\sigma_r^2(r)r}{\sqrt{r^2-R^2}}\mathrm{d}r, \quad (10)$$

$$v^{\bar{4}}_{\rm LOS} = \frac{2}{\Sigma(R)}\int_R^\infty \frac{\nu v^{\bar{4}}_r r}{\sqrt{r^2-R^2}} g(r,R,\beta)\mathrm{d}r \quad (11)$$

$$g(r,R,\beta) = 1 - 2\beta\frac{R^2}{r^2} + \frac{\beta(1+\beta)}{2}\frac{R^4}{r^4},$$

where $\Sigma(R)$ denotes the surface mass density at radius R. As done in Łokas et al. (2005), we will compare the kurtosis

$$\kappa_{\rm LOS} = \frac{v^{\bar{4}}_{\rm LOS}}{\sigma^4_{\rm LOS}}$$

between data and our model.

In the following, we present a non-parametric method for the solution of equation 10 for the total gravitating mass density $\rho(r)$, given tracer density profiles $\nu(r)$ and line-of-sight velocity dispersion $\sigma_{\rm LOS}(R)$. Following **?** we write the overall density profile $\rho(r)$ as

$$\rho(r) = \rho_{\rm DM}(r) + \sum_{i=1}^{N_{\rm pop}}\left(\frac{M_*}{L}\right)_i \cdot \nu_i(r) \quad (12)$$

and assume mass-to-light ratios $(M_*/L)_i$ to be constant with radius for the tracer population i in our mock datasets. We are ultimately interested in $\rho_{\rm DM}$, which is $\rho_{\rm DM}(r) \approx \rho(r)$ when neglecting the mass of the tracer populations. This assumption is valid for our mock data and any observed system with high dark matter content in the center, where the tracer populations reside. We will drop said assumption when working on real data.

We get the enclosed mass $M(<r)$ from the density via

$$M(<r) = \int_0^r \rho(r)r^2\mathrm{d}r, \quad (13)$$

which shows up in eq. 9. In principle, the method can be generalized to investigate alternative gravity models, if the acceleration $GM(r)/r^2$ is replaced with the respective form of $-\partial\Phi/\partial r$ in equation 6.

The degeneracy between mass M and velocity anisotropy β is accounted for: For any non-isothermal system, we let the anisotropy $\beta(r)$ vary as well. We checked that in the case of a simple Hernquist profile, $\beta(r) \approx 0$ is retrieved correctly.

2.1 Representation in Radial Bins

We describe now how we sample the space $[\rho, \nu_i, \beta_i]$ for distinct populations $i = 1...N_{\rm pop}$ of stellar or gaseous tracers. The main idea is to use a representation of the radial profiles of each of those in $N_{\rm bin}$ independent bins,

$$\rho(r_j < r < r_{j+1}) = \rho_j, \qquad \forall j \in [1, N_{\rm bin}], \quad (14)$$

and analogous for ν_i.

The densities ρ and ν_i are represented in terms of the logarithmic density slopes $n(r_j) = -\mathrm{d}\log\rho(r)/\mathrm{d}\log r|r=r_j$, $1 \leqslant j \leqslant N_{bin}+3$, via

$$\rho(r) = \rho(r_{1/2}) \cdot \exp\left[\int_{\log r_{1/2}}^{\log r} n(s)\mathrm{d}s\right],$$

with the density at half-light radius $\rho(r_{1/2}) = \rho_{1/2}$, and $n(r)$ interpolated linearly in between bin radii $r_{j-1} < r < r_j$. We prescribe three fudge $n(r_j)$ for $j \in \{N_{\rm bin}+1, N_{\rm bin}+2, N_{\rm bin}+3\}$ outside of the range where data is given to enable sensible extrapolations towards high radii, and two additional slopes $n_0 < 3, n_\infty > 3$ for the asymptotic density slopes towards $r = 0$ and $r = \infty$, which are reached at half the smallest and $r_\infty = 10$ the largest bin radius.

The velocity anisotropy β is allowed to vary freely in the interval $[0, \infty[$ by sampling the modified, symmetric β_* (**(TODO: cite Read)**),

$$\beta_* = \frac{\sigma_r^2 - \sigma_t^2}{\sigma_r^2 + \sigma_t^2} = \frac{\beta}{2-\beta} \in [-1, 1]$$

with a polynomial

$$\beta_*(r) = \sum_{j=0}^{N_\beta}\beta_j \cdot \left(\frac{r_j}{r_{\rm max}}\right)^j,$$

where $\beta_j \in [0, \beta_{\rm max}]$. With this method, unphysical $\beta > 1$ must be prevented with the correction

$$\beta_*(r_j) := \min(\max(\beta_*(r_j), -1), 1).$$

This approach allows us to change the number of parameters N_β easily, and to sample many qualitatively different models – isotropic, radially biased, tangentially biased, and any gentle transitions between those – with very few parameters.

In a next step, $\sigma_{{\rm LOS},i}(r)$ is calculated from $\rho(r)$, $\nu_i(r)$, and $\beta_i(r)$ according eq. 10. This is done numerically, involving three integrations, which are performed with polynomial extrapolations of the integrands up to infinity, s.t. missing contributions from $r > r_{max}$ do not lead to an artificial falloff of $\sigma_{\rm LOS}$.

The last step involves comparison of the projected surface density $\Sigma_i(r)$ – calculated from the 3D tracer density $\nu_i(r)$ – as well as the LOS velocity dispersion $\sigma_i(r)$, and the fourth order moment of the velocity, if wished, to the respective 2D data profiles for the tracer populations to get a likelihood based on the overall goodness of fit

$$\chi^2 = \sum_{i=1}^{N}\chi^2_{\Sigma,i} + \chi^2_{\sigma,i} + \chi^2_{\kappa,i}, \quad (15)$$

$$\chi^2_{\Sigma,i} = \sum_{j=1}^{N_{\rm bin}}\left(\frac{\Sigma_{{\rm data},i}(r_j) - \Sigma_{{\rm model},i}(r_j)}{\varepsilon_\Sigma(r_j)}\right)^2, \quad (16)$$

with error $\varepsilon_\Sigma(r_j)$ on the data $\Sigma_{\mathrm{data},i}(r_j)$. Analogous expressions hold for $\chi^2_{\sigma,i}$, and $\chi^2_{\kappa,i}$ if used. In absence of a measured $\beta_i(r)$, we set $\chi^2_{\beta,i} = 0$.

2.2 Non-Parametric Representation

There are a large number of parameters from the representation of the profiles,

$$N_{\mathrm{dim}} = N_{\mathrm{bin}} + N_{\mathrm{pop}} \cdot (N_{\mathrm{bin}} + N_{\mathrm{beta}}) \tag{17}$$

with only very few constraints from physical priors. The functional form of the profiles is not predescribed. These conditions is what we call *non-parametric representation*.

2.3 Parameter Space Sampling

Early approaches to sampling the parameter space were performed with a custom-built MCMC method. It proved unfeasible to sample the whole parameter space on human timescales due to its high dimensionality.

To circumvent many likelihood evaluations around a local minimum, we changed the underlying sampling method to use several MCMC walkers, along the lines recently described in (**?**) for their parallel code RUN DMC to analyze radial velocity observations of planetary systems.

A useful framework was found in MultiNest (Feroz et al. (2009)), which is a Bayesian nested sampling algorithm to generate posterior samples from non-trivial distributions in high dimensions.

MultiNest samples the n-dimensional hypercube $\kappa = [0,1]^{N_{\mathrm{dim}}}$, which needs to be translated into physical prior distributions for each of the parameter profiles.

2.4 Priors

Following priors are included in the model, and help to constrain the parameter space to the physically possible range from the start:

1) $0 \leqslant \rho_j \leqslant 6$
2) $0 \leqslant \nu_j \leqslant 6$
3) $0 \leqslant \beta^*_j \leqslant 3$

Additional priors were first included, but then removed later for the following reasons:

1) A baryon prior $\rho(r) \geqslant \rho_b(r) - \epsilon_{\rho,b}(r) \forall r \geqslant 0$, to ensure that no models with overall densities below the measured baryon density are considered any further, can only be used with mock data, where the baryonic density is known to be the sum of the individual tracer densities with known and constant mass to light ratios. This is not the case with real data, where biases towards higher luminosity stars or unaccounted-for populations and gas are missing from the analysis.

2) A mass restriction $M(r > r_{max}) \leqslant M(< r_{max})/3.$, to reject any model which has more than $M_\infty/3$ in the extrapolated bins was introduced to keep the high radius density low, and exclude diverging mass integrals. A more concise approach of requesting $n(r > r_\infty) > n_{\mathrm{thresh}} \geqslant 3$ was chosen, which ensures finite mass toward $r \to \infty$.

3) $\beta_i(r + \Delta r) - \beta_i(r) < 0.5$ to prevent any sudden jumps in β_i is implicitly inherent in the functional setup of β now, when higher order terms are excluded.

3 RESULTS

We apply our method to a set of mock data, in a first run on the spherical models for the Gaia challenge by Walker. They consist of dynamical tracer populations with density distribution

$$\nu_*(r) = \nu_0 \left(\frac{r}{r_*}\right)^{-\gamma_*} \left[1 + \left(\frac{r}{r_*}\right)^{\alpha_*}\right]^{(\gamma_* - \beta_*)/\alpha_*} \tag{18}$$

inside dark matter halos of the form

$$\rho_{\mathrm{DM}} = \rho_0 \left(\frac{r}{r_{\mathrm{DM}}}\right)^{-\gamma_{\mathrm{DM}}} \left[1 + \left(\frac{r}{r_{\mathrm{DM}}}\right)^{\alpha_{\mathrm{DM}}}\right]^{(\gamma_{\mathrm{DM}} - \beta_{\mathrm{DM}})/\alpha_{\mathrm{DM}}} \tag{19}$$

with scale radii r_*, r_{DM}, central slopes of $\gamma_*, \gamma_{\mathrm{DM}}$, transition parameters $\beta_*, \beta_{\mathrm{DM}}$, and outer slopes $\alpha_*, \alpha_{\mathrm{DM}}$.

The anisotropy follows the functional form of **?** and **?**,

$$\beta(r) = 1 - \frac{\sigma^2_\theta}{\sigma^2_r} = \frac{r^2}{r^2 + r^2_a}. \tag{20}$$

with scale radius r_a, turning over from nearly isotropic at $r \to 0$ to radially biased at $r_* = r_a$.

Of these distributions, finite samplings are taken and converted to mock observational data including observational parameters like spectral indices, systemic velocities, proper motions, and binary motions.

3.1 Cusps and Cores

Applied on a profile with a cusp in the DM density profile, $\gamma_{DM} = 1$, our method reproduces the density profile (fig. 1). The further characteristics of the particular mock model are stellar central density slope $\gamma_{*,1} = 0.1, \gamma_{*,2} = 0.1$, stellar turnover slopes $\beta_{*,1} = \beta_{*,2} = 5$, stellar characteristic radii $r_{*,1} = 100\mathrm{pc}, r_{*,2} = 500\mathrm{pc}$, and anisotropy scale radii $r_{a,1} = r_{a,2} = 1.0$. We analyze the data with all tracer particles in one population only first. This population shows a projected tracer half-light radius of $R_{1/2} = 125\mathrm{pc}$.

The shown plots depict the 95 and 68 confidence level (light and dark shaded areas) and the median of all accepted models. The number of models is equal to the number of live points in MultiNest, and is set to twice the number of dimensions, $2 \cdot N_{\mathrm{dim}}$.

The reconstructed profiles for tracer surface density $\Sigma(r)$ and velocity dispersion $\sigma_{\mathrm{LOS}}(r)$ are shown in fig. 2.

The original data is given as a blue shaded region. χ^2 is calculated from the difference between each model's $\Sigma(r)$ and $\sigma_p(r)$, thus the fact that most models are consistent within errors to the data is expected from the low $\chi^2 \leqslant 5$ found after some 1000 iterations.

(TODO: observations for kurtosis) (TODO: link to Tom's papers: kappa does not resolve density/anisotropy degeneracy, Virial Shape Parameters do) (TODO: better/worse fitting of density)

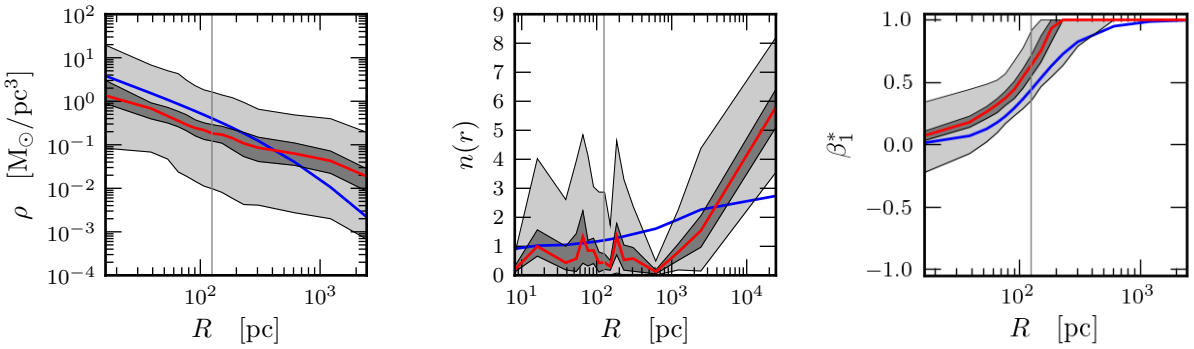

Figure 1. Reconstructed density, density slope, and velocity anisotropy of a cusped model (red shows median, shaded areas are 68 and 95 percentiles) for 10^4 tracer particles, for $3 \cdot 10^5$ models. The blue curve shows the underlying theoretical model. The half-light radius of all stellar tracer particles is depicted as gray vertical line.

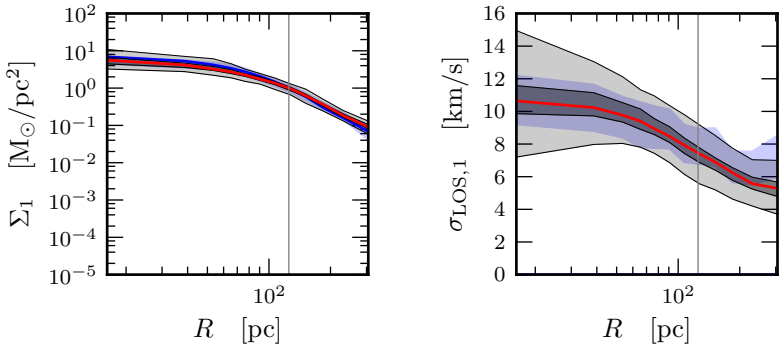

Figure 2. Tracer surface density profile $\Sigma(r)$, normalized to 1 at $r_{1/2}$ and velocity dispersion profile $\sigma_{\mathrm{LOS}}(r)$ for the stellar components in the cusped profile of fig. 1.

3.2 Two populations

The same mock dwarf is analyzed with a model where both populations of tracer particles are accounted for. This is done in the following manner: Each particle in the mock dataset has a number identifying it as a member of population 1, 2, or background. For the plot 3, we used this information directly.

For real data, we will use a splitting based on metallicity. It has been shown for several dwarfs (**(TODO: cite Walker)**) that two or more dynamically distinct populations (**(TODO: what does this mean? how can we tell one star to be in the right population?)**) of stars can be extracted via their metallicity content.

This is achieved by using a separate Markov Chain Monte Carlo method. The overall metallicity distribution is represented by a sum of two Gaussians with means $\mu_{1,2}$ and widths $\sigma_{1,2}$, and each stellar tracer with metallicity M is assigned a population based on the likelihood of its metallicity belonging to said population. The process is repeated to marginalize over the means and widths of the metallicity distributions. A sample splitting result is shown in fig. 4.

(TODO: priors) (TODO: 3 populations?)

3.3 Cored Model

For a cored profile, with $\gamma_{\mathrm{DM}} = 0$, we get the results in fig. 5.

3.4 Triaxial mock data

To test the dependency of GRAVLITE on the assumption of spherical symmetry, we employ it on slightly triaxial mock dwarf galaxies.

The models were generated with the Made2Measure algorithm of **?** and are tailored to follow a similar profile to the profiles specified above for the dwarf galaxies. They show a density profile of

$$\rho(r) = \frac{\rho_S}{\left(\frac{r}{r_S}\right)^\gamma \left(1 + \left(\frac{r}{r_S}\right)^{1/\alpha}\right)^{\alpha(\beta-\gamma)}} \tag{21}$$

with radius r, scale radius $r_S = 1.5$kpc, $\alpha = 1$, $\beta = 4$. For the cusped profiles we have an inner logarithmic slope of $\gamma = 1$, scale density $\rho_S = 5.522 \cdot 10^7 M_\odot/\mathrm{kpc}^3$, and $M_{\mathrm{tot}} = 1.171 \cdot 10^9 M_\odot$, while for the cored one we have $\gamma = 0.23$, $\rho_S = 1.177 \cdot 10^8 M_\odot$, $M_{\mathrm{tot}} = 1.802 \cdot 10^9 M_\odot$. The axis ratios are $b/a = 0.8$ and $c/a = 0.6$. The stars have negligible mass

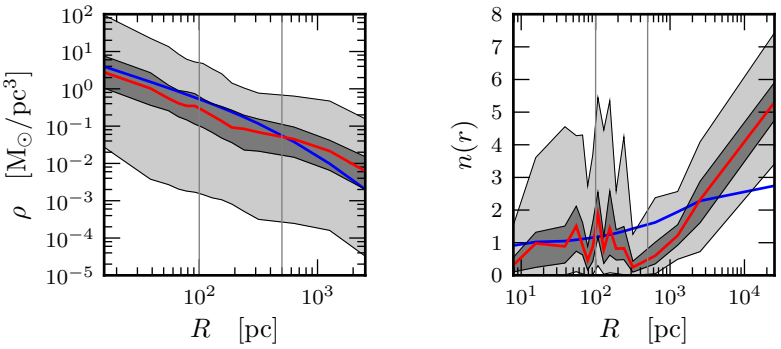

Figure 3. Reconstructed density and density slope for the same cusped model (red shows median, shaded areas are 68 and 95 percentiles) for $2 \cdot 5000$ tracer particles, for $3 \cdot 10^5$ models. The blue curve shows the underlying theoretical model. The half-light radii of the two populations of tracer particles is depicted as gray vertical lines.

Figure 5. A cored profile: Reconstructed mass of the MCMC model (red shows median, shaded areas are 68 and 90 percentiles) for 10^4 tracer particles based on $3 \cdot 10^5$ sampled models. The blue curve shows the underlying theoretical model.

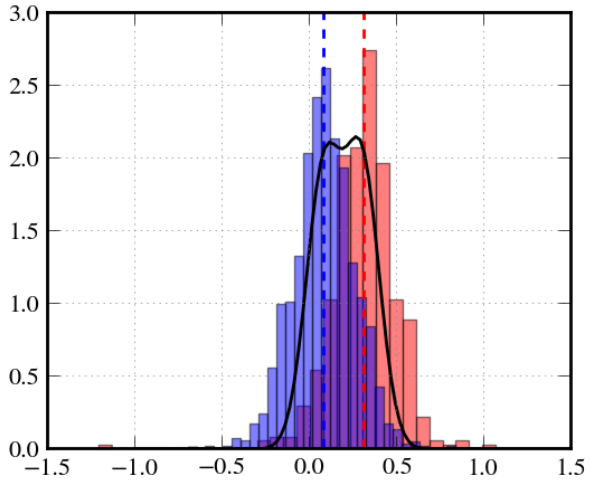

Figure 4. Reconstruction of two populations from mock data. The underlying metallicity distributions are shown as red and blue histograms. The retrieved centers of the Gaussians are shown as vertical lines, and the reconstructed metallicity distribution is depicted as black line.

and follow the same functional form in the density profile as dark matter, with $\alpha = 0.34, \beta = 5.92, \gamma = 0.23, r_S = 0.81$kpc.

The velocity anisotropy of the stellar part is calculated via

$$\beta(r) = \frac{r_{s,\beta}^{\eta}\beta_0 + r^{\eta}\beta_\infty}{r^{\eta} + r_{s,\beta}^{\eta}}, \tag{22}$$

with $r_{s,\beta} = 0.81$kpc, $\beta_0 = 0$, $\beta_\infty = 0.5$ and $\eta = 0.5$, going from isotropic to radially anisotropic with increasing radius.

The retrieved density profile (fig. 6) recaptures the density inside the half-light radius, but constantly overestimates it at $r > r_{1/2}$. This is partly due to projection effects, as the underlying density profile in blue is calculated for spherically averaged density decrease.

4 CONCLUSIONS

The new non-parametric method samples the profiles of the overall density bin-wise, and was shown to reconstruct the density of diverse mock data.

(TODO: better agreement with cusp or with core? what does that tell us?)

The number of bins has to be chosen such that the numerical errors introduced from integrating finite datapoints do not contribute significantly to χ^2. Especially the projection of the 3D model density profiles for the tracer densities onto the 2D plane of the sky introduced was erroneous when done with $N_{bin} \leqslant 7$. Spacing the bins logarithmically instead of setting equal number of tracers per bin helps to circumvent this problem, as does increasing the number of bins. With both approaches, the integral **(TODO: ref.)** includes more of the high density region in the center.

(TODO: minimum data quality needed)

(TODO: Possible contributions to current research.)

5 ACKNOWLEDGEMENTS

JIR would like to acknowledge support from SNF grant PP00P2_128540/1.

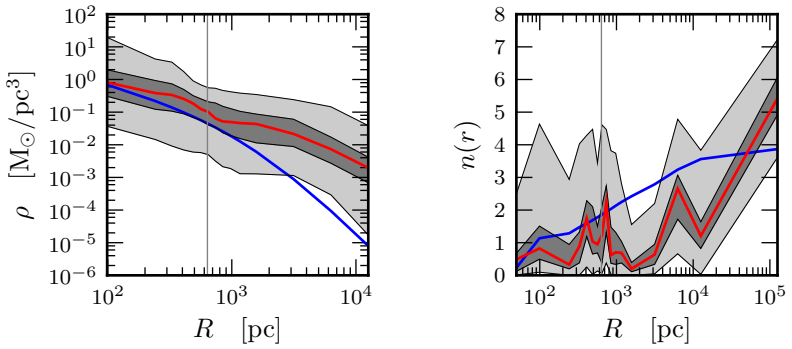

Figure 6. Density profile of a triaxial mock dwarf, for which the line of sight is inclined with 45 degrees with respect to all axes. The vertical line indicates the half-light radius at 640pc.

REFERENCES

Binney J., Tremaine S., 2008, Galactic Dynamics: Second Edition. Princeton University Press

Cole D. R., Dehnen W., Read J. I., Wilkinson M. I., 2012, MNRAS, 426, 601

de Blok W. J. G., McGaugh S. S., Rubin V. C., 2001, AJ, 122, 2396

Feroz F., Hobson M. P., Bridges M., 2009, MNRAS, 398, 1601

Goerdt T., Moore B., Read J. I., Stadel J., Zemp M., 2006, MNRAS, 368, 1073

Governato F. et al., 2010, Nature, 463, 203

Łokas E. L., 2002, MNRAS, 333, 697

Łokas E. L., Mamon G. A., Prada F., 2005, MNRAS, 363, 918

Mateo M. L., 1998, ARA&A, 36, 435

McGaugh S. S., Rubin V. C., de Blok W. J. G., 2001, AJ, 122, 2381

Navarro J. F., Frenk C. S., White S. D. M., 1997, ApJ, 490, 493

Oh S.-H., Brook C., Governato F., Brinks E., Mayer L., de Blok W. J. G., Brooks A., Walter F., 2011, AJ, 142, 24

Read J. I., Pontzen A. P., Viel M., 2006, MNRAS, 371, 885

Schwarzschild M., 1979, ApJ, 232, 236

Spergel D. N., Steinhardt P. J., 2000, Physical Review Letters, 84, 3760

Vogelsberger M., Zavala J., Loeb A., 2012, MNRAS, 423, 3740

Walker M. G., Peñarrubia J., 2011, ApJ, 742, 20